

Flexoelectric switching in cholesteric blue phases

A. Tiribocchi^{*a}, M. E. Cates^a, G. Gonnella^b, D. Marenduzzo^a and E. Orlandini^c

Received Xth XXXXXXXXXX 20XX, Accepted Xth XXXXXXXXXX 20XX

First published on the web Xth XXXXXXXXXX 20XX

DOI: 10.1039/b000000x

We present computer simulations of the response of a flexoelectric blue phase network, either in bulk or under confinement, to an applied field. We find a transition in the bulk between the blue phase I disclination network and a parallel array of disclinations along the direction of the applied field. Upon switching off the field, the system is unable to reconstruct the original blue phase but gets stuck in a metastable phase. Blue phase II is comparatively much less affected by the field. In confined samples, the anchoring at the walls and the geometry of the device lead to the stabilisation of further structures, including field-aligned disclination loops, splayed nematic patterns, and yet more metastable states. Our results are relevant to the understanding of the switching dynamics for a class of new, “superstable”, blue phases which are composed of bimesogenic liquid crystals, as these materials combine anomalously large flexoelectric coefficients, and low or near-zero dielectric anisotropy.

1 Introduction

The blue phases (BPs) of cholesteric liquid crystals provide a remarkable example of soft materials with a rare combination of highly nontrivial geometric and topological nature, and promising technological potential. BPs are three-dimensional networks of disclination lines, which appear due to the spontaneous tendency of a cholesteric liquid crystal to twist along more than one direction. The associated double twist regions lead to topological frustration, as they cannot be used to smoothly tile the three-dimensional space, so that defects, or disclination lines, are unavoidable. In two of the experimentally observed blue phases, BP I and BP II, to which we restrict the present study, such disclinations form ordered lattices, with symmetries characterised by point groups normally with associated crystals (BP III is instead likely amorphous). The spatial period of the disclination lattices is in the submicrometer range, which endows them with interesting optical properties – for instance, a swelling or shrinking of the unit cell would normally be linked to a change in the colour in the sample.

A leap forward in blue phase based technology has been made possible by the stabilisation of these disclination networks over a range of over 60 K, including room temperature^{1–5}. This was a dramatic advance with respect to the previous framework, in which BPs were typically only stable over a fraction of a degree. As a consequence, it has now become

possible to think of blue phases as a possible basis for device or display technology, and this has culminated in the recent fabrication of a blue-phase display device with very fast switching and response times⁶. Such switching times are a natural consequence of the small scale of the unit cells which need to rearrange when a field is applied. Another potential technological advantage of blue phases, which has not been exploited much in practice so far, is that they are associated with a complex and rich free energy landscape, with several competing equilibria which are ideal to build bistable or multistable devices. Such devices can retain memory of two or more states even after the field used to reach these has been switched off (this is a highly sought after property in devices as it leads to huge savings in energy consumption)⁷.

While the stable BPs of Ref. ¹ involved dispersing polymers inside BPs, those of Ref. ³, which provide the main motivation for our current work, were a one-component fluid of “bimesogenic” * liquid crystals, which are associated with very large flexoelectric coefficients⁸. Flexoelectricity in liquid crystals is a linear coupling between applied electric field and induced distortion. This arises, for instance, because the microscopic shape of the molecules (which can be e.g. pear-shaped) allows a coupling between splay (or bend) and polarisation. The treatment of Ref. ⁹ shows that in flexoelectric materials this coupling leads to a renormalisation of the elastic constants, which effectively decrease and facilitates the formation of disclination lines hence of BPs. Conversely, in materials with large flexoelectric coefficients, elastic distortions readily can be created by an external electric field – the flexoelectric coupling is a linear coupling between electric field and order parameter variations, which is allowed in the the-

^a SUPA, School of Physics and Astronomy, University of Edinburgh, Mayfield Road, Edinburgh EH9 3JZ, UK

^b Dipartimento di Fisica and Sezione INFN di Bari, Università di Bari, I-70126 Bari, Italy

^c Dipartimento di Fisica e Astronomia and Sezione INFN di Padova, Università di Padova, Via Marzolo 8, 35131 Padova, Italy

* To form a bimesogenic liquid crystal, one needs a compound which is made up by two polar mesogenic units linked by a flexible spacer⁸.

ory due to the nonsymmetric nature of the molecule. For low enough voltage, this contribution will dominate over the familiar, quadratic, dielectric coupling between order parameter and electric field.

Because any-device oriented application of blue phases is likely to use the stabilised versions of these materials, it is very important to understand the switching behaviour of BPs in response to a flexoelectric, rather than dielectric, coupling to an electric field, as this is likely to be the dominant contribution at least when preparing BP samples as in Ref.³. Therefore, in this work our goal is to elucidate the effect of flexoelectricity in the switching of BP domains, or confined BPs, which can now be potentially used to build real devices. To this end, we use large scale three-dimensional lattice Boltzmann simulations, which have already allowed in the past a careful study of the thermodynamic and flow properties of BPs^{10–14}. Importantly, our approach correctly incorporates hydrodynamic interactions which are known to affect the switching pathway of liquid crystal devices. Our work provides a direct systematic numerical investigation of the switching dynamics of cholesteric blue phases (both in bulk and under confinement) in response to a flexoelectric coupling with the applied electric field (we refer to this phenomenon as “flexoelectric switching”).

This paper is structured as follows. In Section II, we review the free energy density on which the continuum model we use is built, taking care to derive and discuss the extra terms which are due to flexoelectricity and which will play a key role in our work. In Section III we present our results, first focussing on the effect of bulk flexoelectricity on the unit cells of a large BP sample, and then analysing the case of confined geometries. Finally, we draw our conclusion in Section IV, where we also compare the flexoelectric switching studied here with previous works studying response of BPs to a dielectric coupling.

2 Models and methods

2.1 Free energy and equations of motion

In order to investigate the switching properties of flexoelectric blue phases, we consider the formulation of liquid-crystal hydrodynamics given by Beris and Edwards¹⁵, generalized for cholesteric liquid crystals. In this formulation the equations of motion are written in terms of a tensorial order parameter, \mathbf{Q} . The latter is related to the local direction of the individual molecules, $\hat{\mathbf{n}}$, by $Q_{\alpha\beta} = \langle \hat{n}_\alpha \hat{n}_\beta - \frac{1}{3} \delta_{\alpha\beta} \rangle$, where the angular bracket denotes a coarse-grained average and the Greek indices label the Cartesian components of \mathbf{Q} . The tensor \mathbf{Q} is traceless and symmetric and its largest eigenvalue, $2/3q$, ($0 < q < 1$), measures the magnitude of local order. The equilibrium properties of the system are described by a Landau-de Gennes free energy density^{16–18}. This comprises a bulk term

(summation over repeated indices is implied hereafter),

$$f_b = \frac{A_0}{2} \left(1 - \frac{\gamma}{3}\right) Q_{\alpha\beta}^2 - \frac{A_0 \gamma}{3} Q_{\alpha\beta} Q_{\beta\gamma} Q_{\gamma\alpha} + \frac{A_0 \gamma}{4} (Q_{\alpha\beta}^2)^2, \quad (1)$$

which describes a first-order transition from the isotropic to the chiral (cholesteric) phase, together with an elastic contribution which for cholesterics is¹⁷

$$f_d = \frac{K}{2} (\partial_\beta Q_{\alpha\beta})^2 + \frac{K}{2} (\epsilon_{\alpha\zeta\delta} \partial_\zeta Q_{\delta\beta} + \frac{4\pi}{p_0} Q_{\alpha\beta})^2. \quad (2)$$

In the formula above K is the elastic constant (here we are assuming the one-elastic constant approximation) and p_0 is the intrinsic helix pitch of the cholesteric. The tensor $\epsilon_{\alpha\zeta\delta}$ is the Levi-Civita antisymmetric third-rank tensor, A_0 is a constant (with units of pressure) and γ controls the magnitude of order (it plays the role of an effective temperature or concentration according to whether the cholesteric liquid crystal is thermotropic or lyotropic).

To focus on the effect of flexoelectric coupling with an external field E_α , we assume that the liquid crystal has zero dielectric anisotropy and the electric field is uniform throughout the sample. Flexoelectric contributions can be divided into a bulk and a surface one. To account for the former, we add the following term to the free energy density¹⁹:

$$f_E = \epsilon_{fl}^b Q_{\alpha\beta} (E_\alpha \partial_\gamma - E_\gamma \partial_\alpha) Q_{\beta\gamma}, \quad (3)$$

where $\epsilon_{fl}^b > 0$ is the bulk flexoelectric constant. Note that each term of the flexoelectric coupling is linear in E_α and quadratic in \mathbf{Q} . This is different from the standard dielectric coupling where the field couples linearly to the orientational order parameter and quadratically with the electric field. The reduced potential is $V_z = E_z L_z$, where E_z is the component of the electric field along the z -direction and L_z the size of the sample in the same direction.

To describe the anchoring of the director field and the flexoelectric interactions at the boundary surfaces, the following surface contributions are added to the free energy density¹⁷

$$f_s = \frac{W_0}{2} (Q_{\alpha\gamma} - Q_{\alpha\gamma}^0)^2 + \frac{K}{2} [(\partial_\alpha Q_{\beta\gamma})^2 + (\partial_\alpha Q_{\alpha\gamma})(\partial_\beta Q_{\beta\gamma})] + \epsilon_{fl}^s (\partial_\beta Q_{\alpha\beta}) E_\alpha. \quad (4)$$

The first term is a quadratic contribution ensuring a soft pinning of the director field on the boundary surface, along a direction \hat{n}_0 . The parameter W_0 controls the strength of the anchoring and $Q_{\alpha\gamma}^0 = S_0 (n_\alpha^0 n_\gamma^0 - \delta_{\alpha\gamma}/3)$, where S_0 determines the magnitude of surface order. In the strong anchoring regime W_0 is practically infinite so that the director field is effectively fixed at the boundaries. In the weak anchoring regime a term proportional to K , describing the elastic distortion at the surfaces, is also important (see second term in Eq. (4)). Finally,

the flexoelectric contribution at the boundary surfaces is represented by the last term of Eq. (4) where $\epsilon_{fl}^s > 0$ is the surface flexoelectric constant. This contribution depends linearly on the gradients of \mathbf{Q} , and becomes irrelevant in the strong anchoring regime (because the integral of the associated free energy density can be rewritten as a surface integral over the boundary).

It is often convenient to express the free energy in terms of dimensionless quantities. This decreases the number of parameters necessary to describe the system, providing a minimal set on which phase behaviour and electric field effects depend. The parameters are

$$\kappa = \sqrt{\frac{108Kq_0^2}{A_0\gamma}} \quad (5)$$

$$\tau = \frac{27(1-\gamma/3)}{\gamma} + \kappa^2 \quad (6)$$

$$\mathcal{E}_{fl}^b = \sqrt{\frac{E_\alpha E_\alpha (\epsilon_{fl}^b)^2}{A_0 K}} \quad (7)$$

$$\mathcal{E}_{fl}^s = \frac{\epsilon_{fl}^s |E|}{W}. \quad (8)$$

The reduced temperature τ multiplies the quadratic term of the dimensionless bulk free energy, whereas the gradient free energy term is proportional to the chirality κ . This parameter can be considered as a measure of the twist present in the system; it is indeed defined as a ratio between the bulk and the gradient free energies. Lastly, parameters \mathcal{E}_{fl}^b and \mathcal{E}_{fl}^s ¹⁹ measure the strength of bulk and surface flexoelectric couplings. Also notice that in strong anchoring regime W is set to infinity and $\mathcal{E}_{fl}^s \simeq 0$.

The equation of motion for \mathbf{Q} is^{15,20}

$$(\partial_t + \vec{u} \cdot \nabla) \mathbf{Q} - \mathbf{S}(\mathbf{W}, \mathbf{Q}) = \Gamma \mathbf{H} \quad (9)$$

where Γ is a collective rotational diffusion constant. The first term of the left hand side of Eq. (9) is the material derivative describing the usual time dependence from advection by a fluid with velocity \vec{u} . For the tensor field \mathbf{Q} , this is generalized by the term¹⁵

$$\begin{aligned} \mathbf{S}(\mathbf{W}, \mathbf{Q}) &= (\xi \mathbf{D} + \omega)(\mathbf{Q} + \mathbf{I}/3) + (\mathbf{Q} + \mathbf{I}/3)(\xi \mathbf{D} - \omega) \\ &- 2\xi(\mathbf{Q} + \mathbf{I}/3)\text{Tr}(\mathbf{Q}\mathbf{W}) \end{aligned} \quad (10)$$

where Tr denotes the tensorial trace, while $\mathbf{D} = (\mathbf{W} + \mathbf{W}^T)/2$ and $\omega = (\mathbf{W} - \mathbf{W}^T)/2$ are the symmetric and the anti-symmetric part of the velocity gradient tensor $W_{\alpha\beta} = \partial_\beta u_\alpha$. The presence of $\mathbf{S}(\mathbf{W}, \mathbf{Q})$ is due to the fact that the order parameter distribution can be both rotated and stretched by the fluid. This is a consequence of the rod-like geometry of the LC molecules. The constant ξ depends on the aspect ratio of the

molecules forming a given liquid crystal and controls whether the director field is flow-aligning in shear flow ($\xi \geq 0.6$ for $\gamma = 3$), creating a stable response, or flow-tumbling, which gives an unsteady response ($\xi \leq 0.6$ for $\gamma = 3$). The term on the right-hand side of Eq. (9) describes the relaxation of the order parameter towards the minimum of the free energy. The molecular field \mathbf{H} which provides the driving motion is given by

$$\mathbf{H} = -\frac{\delta \mathcal{F}}{\delta \mathbf{Q}} + (\mathbf{I}/3)\text{Tr}\frac{\delta \mathcal{F}}{\delta \mathbf{Q}}. \quad (11)$$

with \mathbf{I} being the unit matrix and \mathcal{F} the free energy.

The three-dimensional fluid velocity, \vec{u} , obeys the continuity equation,

$$\partial_t \rho + \partial_\alpha (\rho u_\alpha) = 0 \quad (12)$$

and the Navier-Stokes equation,

$$\rho(\partial_t + u_\beta \partial_\beta) u_\alpha = \partial_\beta (\Pi_{\alpha\beta}) + \eta \partial_\beta (\partial_\alpha u_\beta + \partial_\beta u_\alpha), \quad (13)$$

where ρ is the fluid density and η is an isotropic viscosity. Note that the form of this equation is similar to that for a simple fluid. However, the details of the stress tensor, $\Pi_{\alpha\beta}$, reflects the additional complication of cholesteric liquid crystals hydrodynamics. This tensor is explicitly given by:

$$\begin{aligned} \Pi_{\alpha\beta} = & - P_0 \delta_{\alpha\beta} + 2\xi(Q_{\alpha\beta} + \frac{1}{3}\delta_{\alpha\beta})Q_{\gamma\epsilon}H_{\gamma\epsilon} \\ & - \xi H_{\alpha\gamma}(Q_{\gamma\beta} + \frac{1}{3}\delta_{\gamma\beta}) - \xi(Q_{\alpha\gamma} + \frac{1}{3}\delta_{\alpha\gamma})H_{\gamma\beta} \\ & - \partial_\alpha Q_{\gamma\epsilon} \frac{\delta \mathcal{F}}{\delta \partial_\beta Q_{\gamma\epsilon}} + Q_{\alpha\gamma}H_{\gamma\beta} - H_{\alpha\gamma}Q_{\gamma\beta}. \end{aligned} \quad (14)$$

Here P_0 is an isotropic background pressure.

2.2 Numerical set up and mapping to physical units

In this section we briefly describe the numerical aspects of our work.

The size of the simulation box is equal to $L_x = 32, L_y = 32, L_z = 32$ lattice sites. Note that the size of the unit cell which minimises the free energy is in general different from (and typically larger than) the cholesteric pitch. Because we can only simulate an integer number of periodic unit cells within a periodic simulation domain, in order to account for this extra degrees of freedom we employ the following procedure. Keeping fixed the size of the periodic domain, we rescale the size of the simulation box by a factor called “red-shift”^{† 22–24}. In simulations with periodic boundaries in all directions, we have followed the recipe proposed in Ref.¹⁹,

[†] This name refers to the shift, towards longer wavelengths, of the BPI Bragg back reflection with respect to that of the cholesteric phase²¹. In other words, the unit cell size of the blue phase is typically larger than the cholesteric half pitch.

in which the redshift is calculated at every time step by minimizing the free energy. Since the free energy functional comprises terms up to quadratic order in gradients of \mathbf{Q} , a rescaling of the unit cell dimension, $K \rightarrow K/r$ (with r the redshift), modifies the gradient terms, that are in turn rescaled by a factor of r per derivative. The free energy can be rewritten as $f(\mathbf{Q}) = r^2 a(\partial \mathbf{Q}^2) + r b(\partial \mathbf{Q}) + c$, and the rescaling factor r^* that minimizes the free energy is $r^* = -b/2a$. In particular we assume a single redshift governing all the three dimensions¹⁰. We found that the presence of redshift does not affect the switching dynamics of BP cells¹². In simulations with homeotropic or homogenous anchoring, the redshift was set to one to avoid any change in the size of the confining cell. According to the experience gained in the bulk simulations, allowing for a finite redshift can lead to quantitative, but not qualitative, differences in the dynamics.

The equilibrium structures of BPI and BPII in the absence of any field were obtained by relaxing the free energy to its minimum value by numerically solving Eq. (9). Initial configurations were set according to the approximate solutions given in Ref.¹⁶, where it was shown that the topological character of the equilibrium defect structure at high chirality (where the bulk and the external field free energy terms become negligible compared to the gradient free energy and an analytical solution is possible) is retained by reducing the chirality. These solutions are taken as initial conditions for the dynamic equations²² (9), (12) and (13) that are numerically integrated by using an hybrid scheme in which standard lattice Boltzmann methods¹¹ are used to update the Navier-Stokes equation while Eq. (9) is solved by using finite difference scheme based on a predictor corrector algorithm. This approach has been already successfully tested for other systems such as binary fluids^{25–27}, active nematics^{11,28} or blue phases¹². A typical simulation reported in this work was run in parallel on 8 nodes with MPI architecture, and required about 5 days to be completed.

In our calculations we fixed $\Gamma = 0.3$, $\xi = 0.7$ and $\eta = 1.333$ as in previous numerical works^{12,22}. We have also set $A_0 = 0.00308$, $K = 0.005$, $\gamma = 3.775$ for BPI, and $A_0 = 0.00075$, $K = 0.005$, $\gamma = 3.086$ for BPII. This choice guarantees we are in the correct region of the phase diagram²². In order to get from simulations to physical units we follow the approach of Refs.^{13,29}. Our parameters correspond to a blue phase with length scale fixed by the cholesteric pitch p_0 , typically in the range of 100 – 500nm¹⁶, and (Frank) elastic constants equal to ~ 10 pN and ~ 16 pN for BPI and BPII respectively, as for a typical liquid crystalline material. One space and time LB unit correspond to 0.0125 μm and 0.0013 μs for BPI, and to 0.0125 μm and 0.0017 μs for BPII, with a rotational viscosity equal to 1 Poise. The mapping of flexoelectric couplings can be done by matching the previously defined dimensionless quantities, \mathcal{E}_{fi}^b and \mathcal{E}_{fi}^s , when defined in simulation and

in physical units. For instance, for BPII a value of $\mathcal{E}_{fi}^b = 0.3$ (which is in the middle of the range used in our runs) corresponds to a system with (Frank) elastic constants equal to ~ 10 pN as before, with a value of $\epsilon_{fi}^b \sim 10$ pC/m, subject to a field of ~ 15 V/ μm . These values are typical of liquid crystal devices; to directly apply our results to this situation, we further need to select a liquid crystal for which dielectric effects are negligible, which is challenging at these field strengths – a possibility is to use bimesogenic materials which have near-zero dielectric anisotropy. On the other hand, a value of the dimensionless surface flexoelectric coupling of $\mathcal{E}_{fi}^s = 0.15$ may correspond to the same BPII material, when the anchoring at the surface is $W \sim 0.0007$ N/m. For BPI, a similar mapping applies.

Finally, to locate the defects in the simulation domain, we used the approach described in¹², where a lattice point is considered to belong to a defect if the local order at that point assumes values below a given threshold. Here the threshold is fixed to be 60% of the largest eigenvalue of \mathbf{Q} in the bulk (i.e. away from all defects).

3 Results

3.1 Flexoelectric effects in blue phase samples with periodic boundary conditions

We now discuss the results obtained by looking at the switching dynamics of BPI and BPII unit cells with periodic boundary conditions. We will focus on the deformations of the defect structure observed when a field is applied to the sample along the z -direction ($[0, 0, 1]$ direction), only considering the effect of bulk flexoelectric couplings. The surface flexoelectric contribution vanishes with these boundary conditions, and the dielectric contribution is disregarded to focus on flexoelectricity. For comparison, a single case in which the field is along the diagonal of the unit cell ($[1, 1, 1]$ direction) will be also considered, to get a feel for the anisotropy of the response.

BPs are arranged in a $L_x = L_y = L_z = 32$ periodic unit cell. The initial equilibrium defect structures (see Fig.1a for BPI and Fig.3a for BPII) are obtained by minimizing the free energy by using exclusively the evolution equation Eq. (9)^{12,22}. Notice that in this case the minimization is driven exclusively by the molecular field \mathbf{H} . Unless otherwise stated, hydrodynamic interactions are switched on after this equilibration, and remain in place throughout the dynamical switching simulations.

Fig.1 shows the response of a periodic BPI unit cell under a bulk electric field applied along the z -direction. The field strength chosen ($\mathcal{E}_{fi}^b \simeq 0.5$) is large enough to modify the initial defect structure in an appreciable way. When the field is switched on, disclinations start to bend and twist, although the typical BPI defect structure is still recognizable

(Fig.1b). As time goes on these defect distortions become more and more pronounced resulting into strongly bent arcs that span the entire unit cell and are aligned along the direction of the field (Fig.1c). Later arcs reorganize to form “X-like” defect junctions (Fig.1d) that successively unbind at their center (Fig.1e) giving rise to columnar-like disclinations parallel to the z -direction (Fig.1f). Fig.1 shows that the flexoelectric switching dynamics under a strong field is extremely different from previously studied cases in which only dielectric effects have been considered^{12,30}. In the latter case the disclinations twist (for small field) or reconnect to lead to an amorphous state, in stark contrast with the regular structures of parallel defect lines obtained here. For lower fields (provided these are still high enough to break the defect structure), the field-induced states are characterized by the same defect network, with the typical hexagonal pattern for the director profile. Interestingly, for those cases, during the switching on dynamics, double helical disclinations are observed initially, perpendicularly to the direction of the applied field – these later on merge and reorganize into the column-like pattern. Similar textures have already been described in Ref.²³ as intermediate field-induced states, while in our simulations these are only transient defect structures. These differences might be due to different values of bulk and elastic constants considered (for example, the theoretical description in²³ relaxes the one elastic constant approximation).

A crucial point in the physics of devices is the understanding of the switching off dynamics, i.e. the time evolution of the system when the field is switched off. In particular one would like to answer the following question: Is the device switchable (i.e. does it recover the initial defect structure when the field is removed), or does it get stuck into a metastable state characterized by a different defect network? In our experiment, as the flexoelectric coupling is switched off, the disclination lines start to bend, approach one another (Fig.1g), and merge into a connected structure that is similar in shape to the “X-like” state observed during the switching on dynamics but with thinner disclinations (Fig.1h). Later on defects reorganize themselves into arcs that first span the entire system (Fig.1i), then gradually stretch (Fig.1j) and finally split forming long undulated defect lines (Fig.1k and l), some of them in proximity of the center of unit cell, others closer to the boundaries.

As Fig. 1 clearly shows, the system cannot recover the initial state of Fig.1a, but it gets stuck into a metastable state (see Fig. 1l) whose free energy is higher than the initial one. On the other hand this design can be still considered as a switchable device since further simulations show that there exists a reversible cycle between the field-induced state in Fig. 1f and the metastable state in Fig. 1l. It is interesting to look also at the director profile of the state of Fig.1f induced by the flexoelectric coupling. In Fig.2 this is shown for a cross section in the xy plane taken at $L_z/2$: the structure consists of an

hexagonal lattice of defects of $-1/2$ topological charge that separate regions of splay-bend distortions around a line passing through the center of the hexagon (i.e., the disclination in three dimensions). This spatial organization of the defects is in agreement with what found in Refs.^{19,31}, where a similar structure has been identified as a stable configuration of the director field, for either a spontaneously splayed nematic liquid crystal or a blue phase under an intense electric field, respectively. We find here that this state is naturally found in blue phases with flexoelectricity, and hence should be particularly relevant for the stabilised BPs recently found experimentally in Ref.³.

A different kinetic pathway is observed when a field (still along the z -direction with $\mathcal{E}_{fl}^b \simeq 0.5$) is applied on a BPII structure with periodic boundary conditions (see Fig.3). With respect to the BPI case the effect of the field is less dramatic and the typical (zero field) BPII network of defects is still recognizable even when the field is on. The persistence of a structure resembling (or topologically connected with) that of zero field, arguably suggests that the device should switch back to BPII when the field is taken off. This is indeed what happens. More precisely, when the field is switched on, the defect structure is initially bent and twisted at its center, while the regions in which the director field is distorted around a defect line widens (Fig.3b). The latter effect is made apparent by looking at the effective thickness of the disclination tubes. The device is driven towards a field induced state characterised by a defect structure similar to the zero-field (equilibrium) one (the shift along the z -direction is immaterial in view of the periodic boundary conditions, see Fig.3c). When the field is switched off, the disclination profile remains essentially undistorted, with only a progressive slow reduction of the thickness of the defects (Fig.1d and e) until the typical zero-field BPII structure (shifted along the z -direction) is recovered. Notice that only one cycle is here necessary to restore the initial defect pattern.

We now look at the dependence of the defect dynamics with respect to the direction of the applied field. In Fig.4 we report the time evolution of the defect network of BPI when a field is applied along the diagonal of the unit cell direction $([1, 1, 1])$ which is not related to $[0, 0, 1]$ by the cubic symmetry of the structure. Similarly to the case with the field along the z -direction, the strength of the applied field is large enough to significantly rewire the defect network. The steady-state field-induced state still has the defect lines broadly aligned along the field, but not as markedly as in the $[0, 0, 1]$ case. When the field is switched off, the device gets again stuck in a metastable configuration, different than the one obtained when removing the field along the $[0, 0, 1]$ direction.

Intriguingly, we find the switching-on dynamics depends strongly on field direction, and in all cases proceeds via multiple steps visible in the transient plateaus observed in the plots

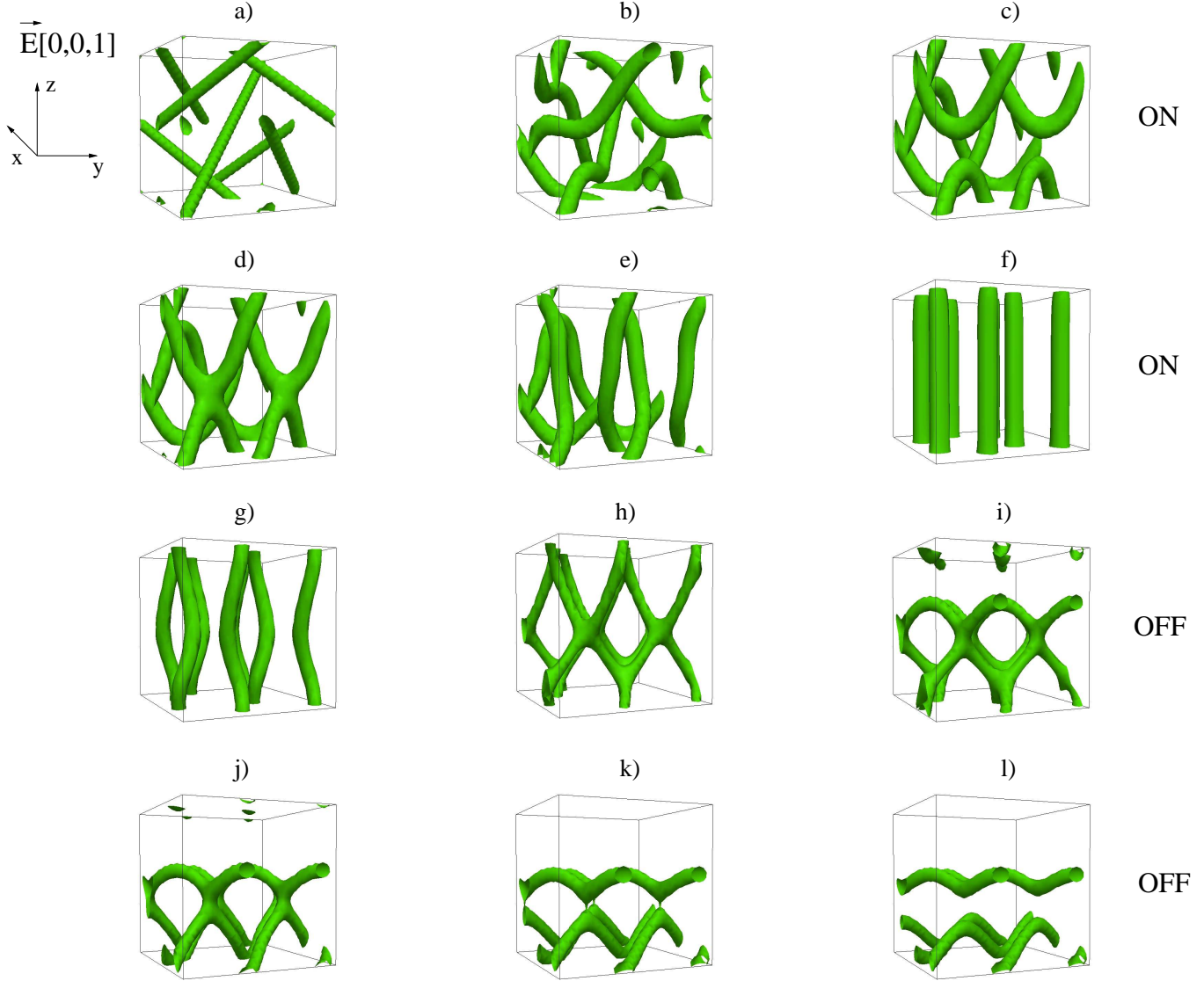


Fig. 1 Defect dynamics of the BPI phase during the switching on (a) – f)) -off (g) – l)) in a simulation box of size $32 \times 32 \times 32$. Periodic boundary conditions are set in all directions. The electric field, applied along the z-direction ($[0, 0, 1]$), is $\mathcal{E}_{ff}^b \simeq 0.5$. It is switched off at $t = 100 \times 10^4$. One cycle is not enough to have a switchable device. A further application of the field reveals the device is switchable between the states f) and l).

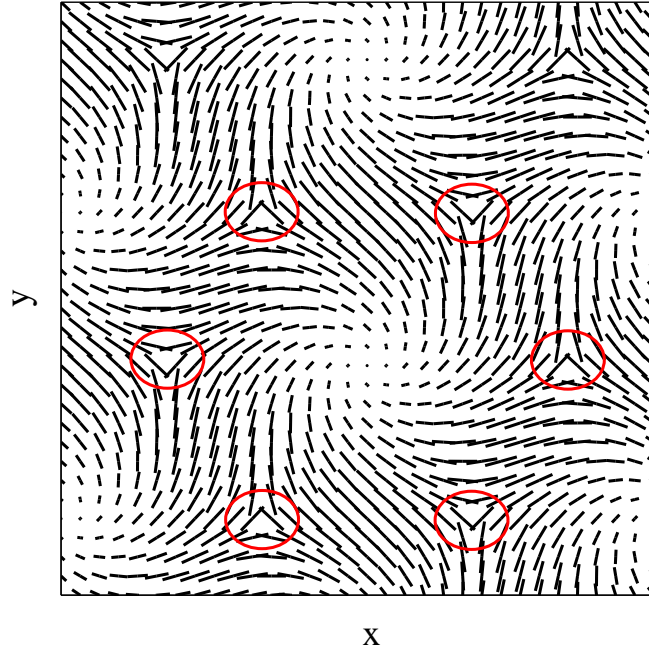


Fig. 2 Director profile on the xy plane taken at $L_z/2$ of the metastable state f) of Fig.1. Red circles indicate the presence of a charge $-1/2$ topological defect.

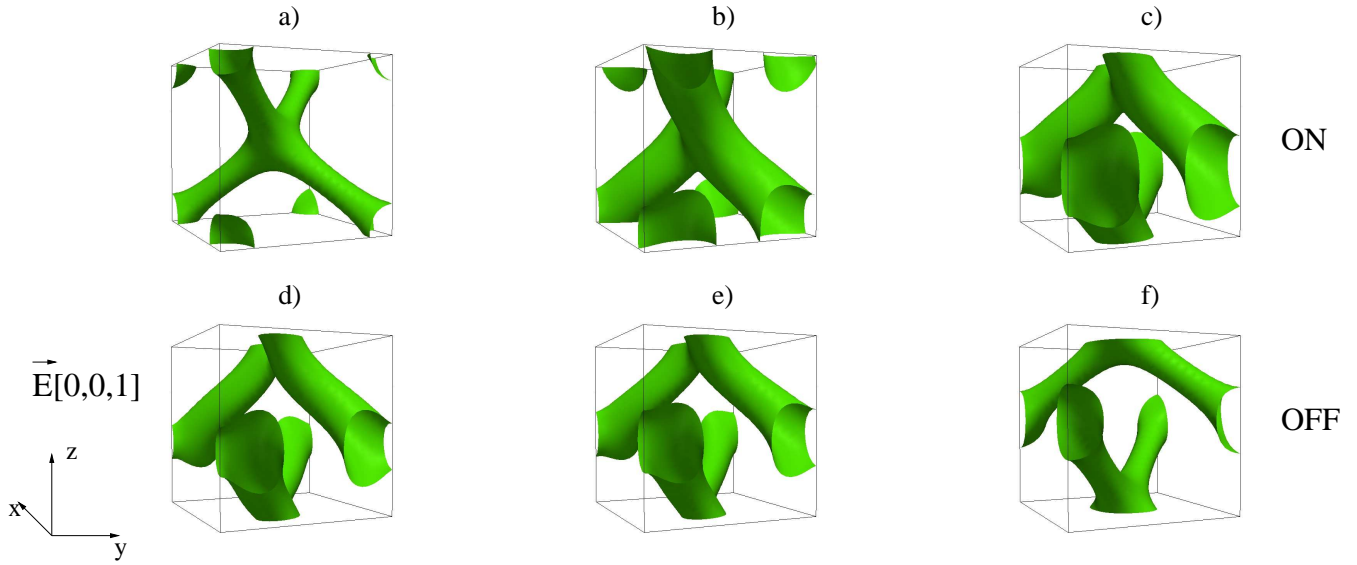


Fig. 3 Switching defect dynamics of a BPII phase of unit cell size $32 \times 32 \times 32$ with periodic boundary conditions along all directions. The electric field, applied along the z -direction ($[0, 0, 1]$), is $\mathcal{E}_{fl}^b \simeq 0.5$ (from a) to c). It is switched off at $t = 80 \times 10^4$ (from d) to f). After one cycle, the system recovers the initial disclination structure (shifted along the z -direction), making the system switchable.

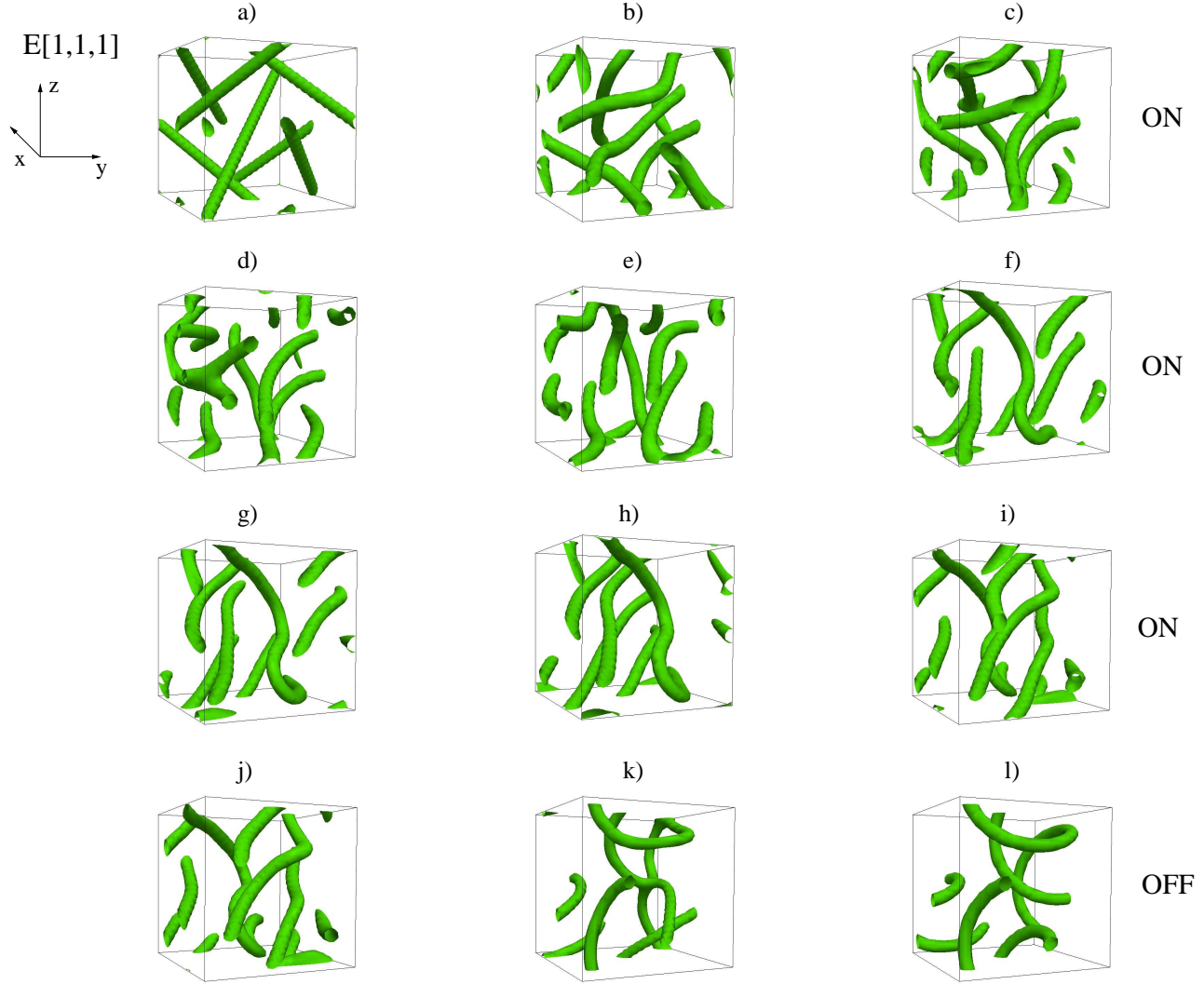


Fig. 4 Evolution of the disclination network of the BPI phase during the switching on (*a*) – (*c*)) -off (*d*) – (*f*)) dynamics in a simulation box of size $32 \times 32 \times 32$ with periodic boundary conditions in all directions. The electric field, applied along the diagonal direction $[1, 1, 1]$, is $\mathcal{E}_{fl}^b \simeq 0.5$. It is switched off at $t = 60 \times 10^5$. When the field is on, the device is driven towards a metastable state. When the field is removed again a metastable state featuring twisted disclinations is attained.

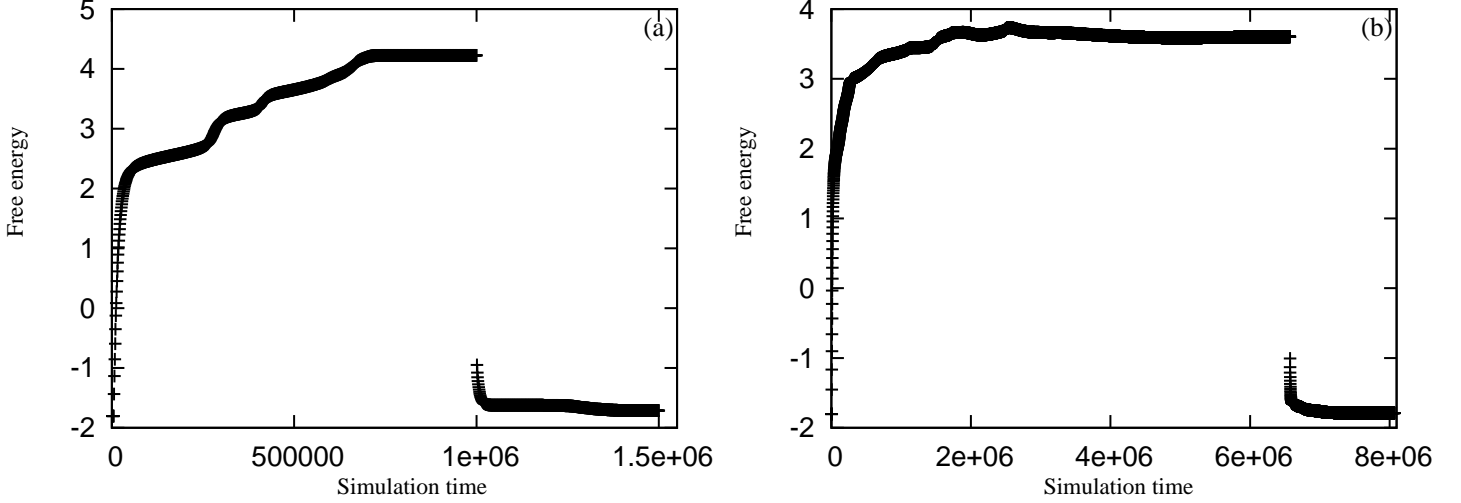


Fig. 5 Time evolution of the free energy in a BPI unit cell during a switching on-off dynamics with an electric field applied along the z -direction ($[0,0,1]$) (plot (a)) and along the diagonal direction ($[1,1,1]$) (plot (b)). The field is $\mathcal{E}_{fl}^b \simeq 0.5$ in both cases. Interestingly the time evolution of the diagonal field case is ~ 6 time longer than the case in which the field is along the z -direction. (These free energy curves correspond to runs without hydrodynamics. This omission allows us to reach a larger value of the electric field, which emphasises the differences in the dynamics, avoiding at the same time numerical stability issues).

of the free energy versus time (see Fig. 5).

3.2 BP samples under confinement

We now turn to the switching dynamics of a field in confined BP samples. These are particularly relevant to real-world devices, as these necessarily include boundaries, where the director field can easily be anchored, either chemically or mechanically via rubbing – and the anchoring strength can often be controlled. In this Section we will only focus on BPI cells, which, as shown in the previous Section, lead to a more interesting dynamics in the bulk. We consider either homeotropic (normal) or homogeneous (planar) anchoring on upper and lower walls, and periodic boundary conditions in other directions. To better compare with the results discussed previously, the size of the simulation box is set to $32 \times 32 \times 32$. The field is then applied along the z -direction ($[0,0,1]$). Once more, its magnitude is strong enough that the initial defect network breaks up. The case of a surface flexoelectric coupling is also explored below – in this case the field effects are confined to the boundaries.

The presence of confining surfaces strongly affects the stability of defects in liquid-crystalline systems. In previous numerical studies^{32,33}, the existence of several defect structures (sometimes described as “exotic” structures), very different from that of the equilibrium BPI cell, have been proposed. A parallel array of double-helical disclinations, and two sets of undulating defect lines, were observed in a cell with homeotropic anchoring on both (parallel and flat) walls,

when their distance was of the order of the helical pitch³². On the other hand, ring defects structures emerge when homogeneous anchoring is set on both walls³³. A key question, crucial for devices, concerns how to dynamically switch among different metastable states to kinetically reach, in a controlled way, a target structure. Recent studies¹² on the switching defect dynamics showed that applied electric fields could represent an interesting route to reveal the existence of even more metastable states. A simple switching on-off schedule can lead, for example, to a bistable defect network¹⁴, where each state is uniquely selected by the application of the electric field along an appropriate direction. Interestingly, some key questions arise when flexoelectric in confined samples is taken into account. What is the switching dynamics? Is this affected by the choice of different boundary conditions?

To address these issues, in Fig.6 we show the flexoelectric switching of a BPI cell with homeotropic anchoring (with a slight pretilt of $\sim 10^\circ$ from the z -direction) on both walls. We have also set $\mathcal{E}_{fl}^b \simeq 1$ (applied along the z -direction) and $W_0 = 0.1$, which still corresponds to moderately strong anchoring.

The first thing to note is that the equilibrium defect structure (Fig.6a) is different from the typical one observed for the BPI at equilibrium with periodic boundaries, although the basic BPI topology is still recognisable (for instance in the disclinations in the interior of the cell). This metastable structure is the same as that reported in Refs.^{14,32}. A second, key, observation is that the dynamics of flexoelectric switching are significantly affected by the anchoring. Thus, the normal an-

choring conditions in Fig. 6 lead to a visible initial bend of the diagonal disclination. This is followed later on by the formation of straight defect lines as in the bulk case (see Fig. 6b and c), which branch out at the boundary to end up parallel to the confining planes there (see Fig. 6d–f). Once more, upon field removal the system drifts away from the field-induced state in Fig. 6f into another metastable state, featuring undulating defect lines close to but distinct from those observed in the bulk (compare Fig. 6i with Fig. 11).

Homogeneous boundary conditions, as can be achieved by rubbing the liquid crystal at the boundaries, lead to yet different structures in equilibrium, and to new kinetic pathways during switching on and off a field. The behaviour of a BPI cell with such planar anchoring (along the x direction) is shown in Fig. 7. The flexoelectric coupling is again given by $\mathcal{E}_{fl}^b \simeq 1$, and the anchoring $W_0 = 0.1$ as in Fig. 6. The equilibrium defect network is now made up of an array of isolated twisted ring disclinations located in the bulk of the device (Fig. 7a). These structures have already been discussed in Ref.³³ and, as a field induced state, in the bistable BP device proposed in Ref.¹⁴: we do not dwell on them here, and rather focus on the field-induced aspects. When the field is switched on, the network is initially bent and stretched (Fig. 7b and c) with disclinations again aligning parallel to the field until they touch the walls. Later on they recombine into elongated rings now connected to defects pinned up at the walls ((Fig. 7d, e and f). As in the previous cases, when the field is removed defects depin from the surfaces and form connected ring arcs in the bulk (from Fig. 7g to j). Then the network develops branching points which are unstable and annihilate in the bulk leaving a state with arcs of defects spanning the whole device (Fig. 7k and l).

Lastly, we investigate the switching dynamics in response to surface flexoelectricity. For strong anchoring these contributions can be rewritten as surface terms, so one may expect that their presence may only lead to deviations from the equilibrium bulk disclinations in strongly confined samples, such as the ones we are considering. As we mentioned previously, because the field couples with the derivative of the order parameter (see Eq. 4), in the case of strong anchoring the coupling is identically zero at the boundaries and the surface flexoelectric term is not effective. However for finite anchoring (as the case of $W_0 = 0.1$ we consider), this is not true anymore, and the director can deviate from the anchoring direction, at the cost of some surface energy.

To address the role of the surface flexoelectric coupling, we simulated the evolution of disclinations in a confined BPI cell with homogeneous anchoring (Fig. 8). The magnitude of the field, applied along the z -direction, is such that $\mathcal{E}_{fl}^s \simeq 0.15$ (a pretilt of $\sim 10^\circ$ from the plane is also included). Now the switching leads to a shrinkage and eventual annihilation of the twisted disclination loops (the full kinetic pathway is

shown in Fig. 8a–i). The final state is defect-free (Fig. 9), and the associated director profile has a lot of splay-bend deformations. Intriguingly, this state is similar to the spontaneously splayed nematics in an achiral liquid crystal with a strong flexoelectric coupling, predicted in¹⁹. As expected, the state remains disclination free even when the field is removed.

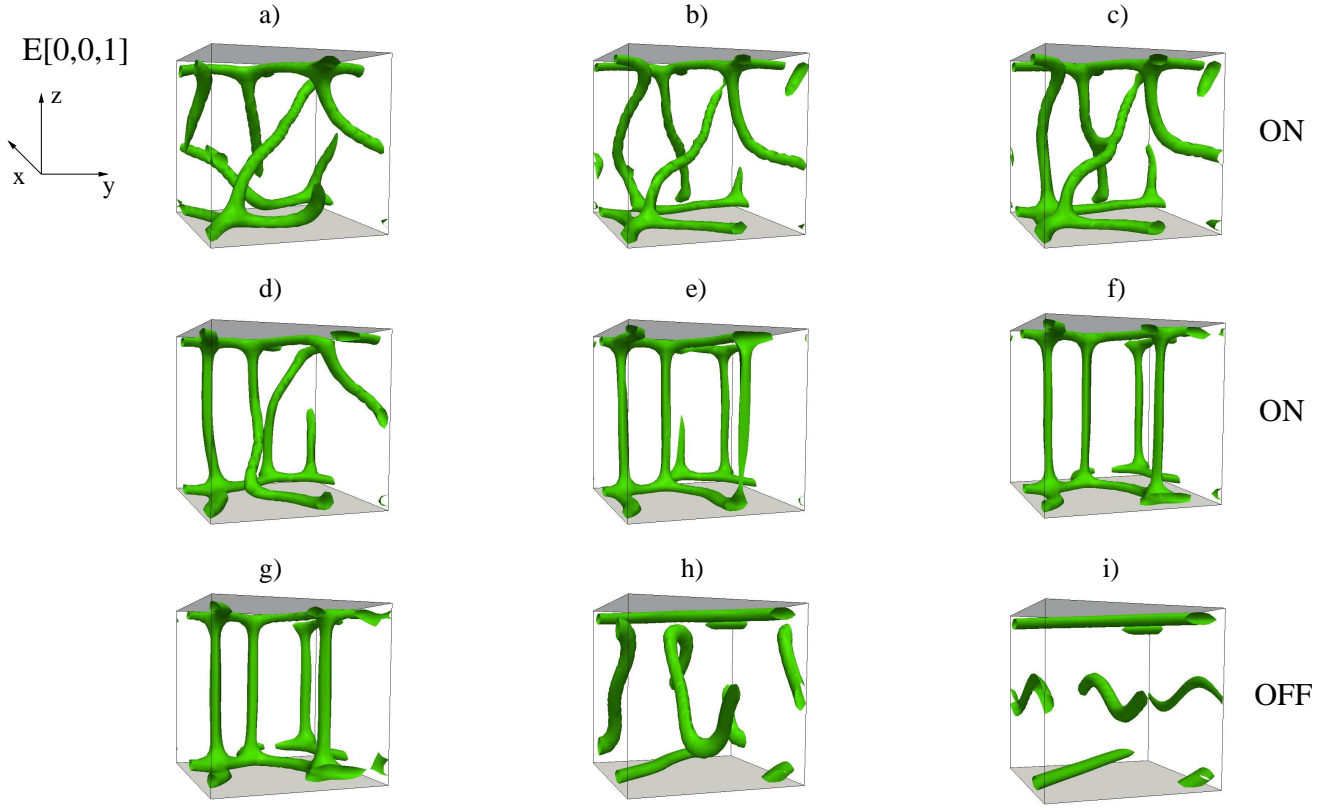
4 Conclusions

To summarise, we have numerically investigated the switching dynamics of cholesteric blue phases in the presence of a flexoelectric coupling with an electric field. The choice of boundary conditions (periodic boundaries, or confined samples with homogeneous or homeotropic anchoring on both walls) and of the dynamical schedule of the field application crucially affect the dynamics, yielding several intriguing defect structures. Some of these resemble the zero-field equilibrium network (e.g. for BPII), while others organize forming novel field induced stable or metastable states. The most frequently observed structure is one where the disclinations are aligned (more or less markedly, according to the different cases) along the field direction.

With periodic boundary conditions (corresponding to the bulk of a large sample) and with a field applied along the $[0, 0, 1]$ direction, BPI defects align along the direction of the applied field via a complex kinetic pathway which includes the formation of intermediate “X-like” disclination junctions. Once the field is switched off, the network is stuck in a zero-field metastable state. Remarkably, a further application of the field restores the field induced states, thereby making these cells switchable. When the field is applied along the $[1, 1, 1]$ direction, the alignment is imperfect and the dynamics is slower.

Importantly, in both cases, as for most of the other geometry/boundary condition choices, upon switching off, the field-induced BPI structure drifts away from the field-induced conformation and gets stuck into a metastable phase, the details of which depend on boundary conditions, field directions etc.. This means that, while the field-aligned disclination state is switchable, it cannot, at least under the conditions explored by our simulations, be used as the basis for multistable energy-saving devices such as those described in¹⁴. (However we have laid the formulation for future computational searches for these). The inability to reform an equilibrium BPI structure also suggests that large memory effects are present.

Confined samples lead to qualitatively different results. With normal, or homeotropic, anchoring at the boundaries, and bulk flexoelectric coupling only, the field-aligned disclinations branch at or close to the wall to end up parallel to the boundaries there. With homogeneous anchoring the defects without a field form twisted rings; these elongate and align with the field when bulk flexoelectricity is switched on. Sur-



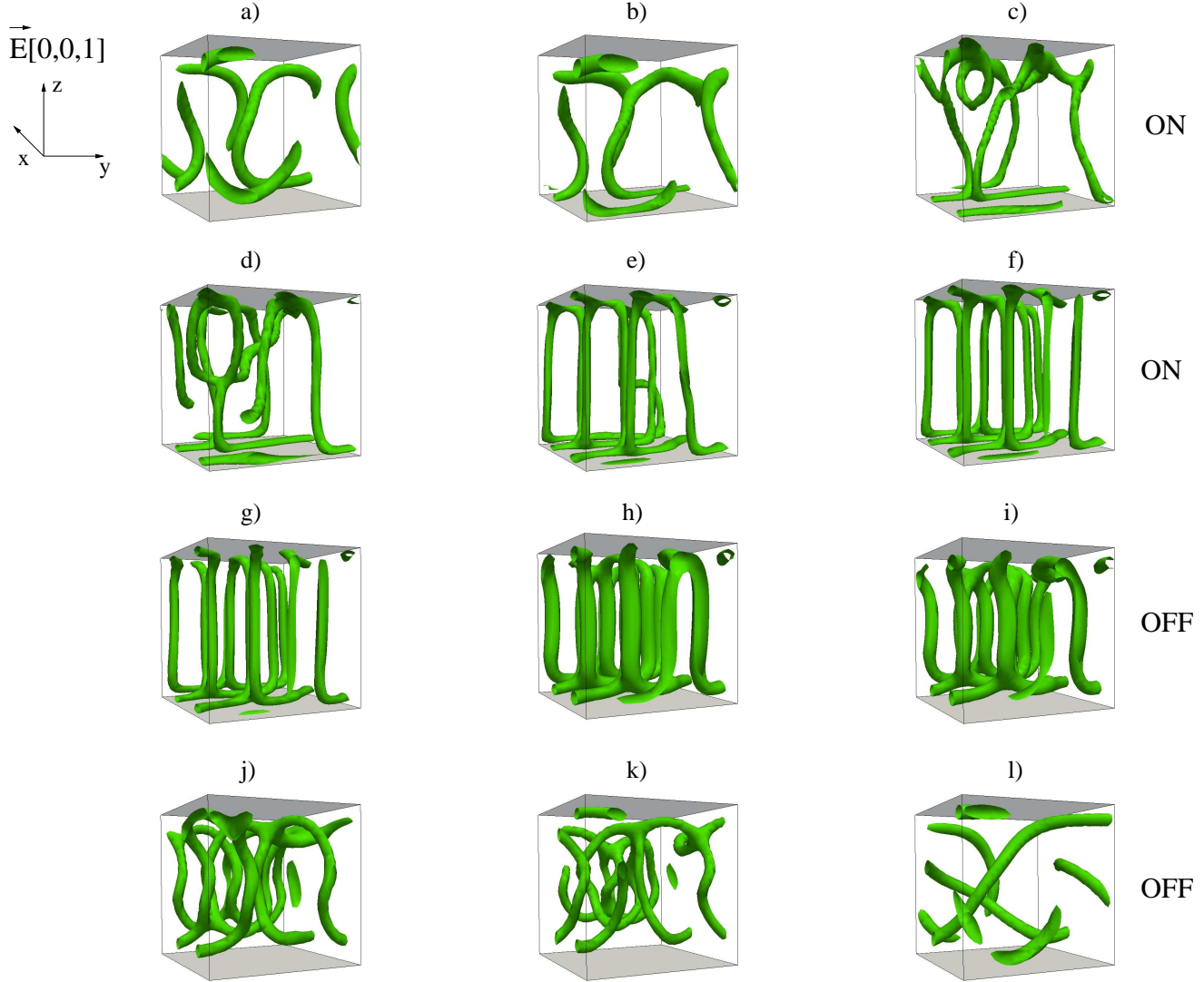
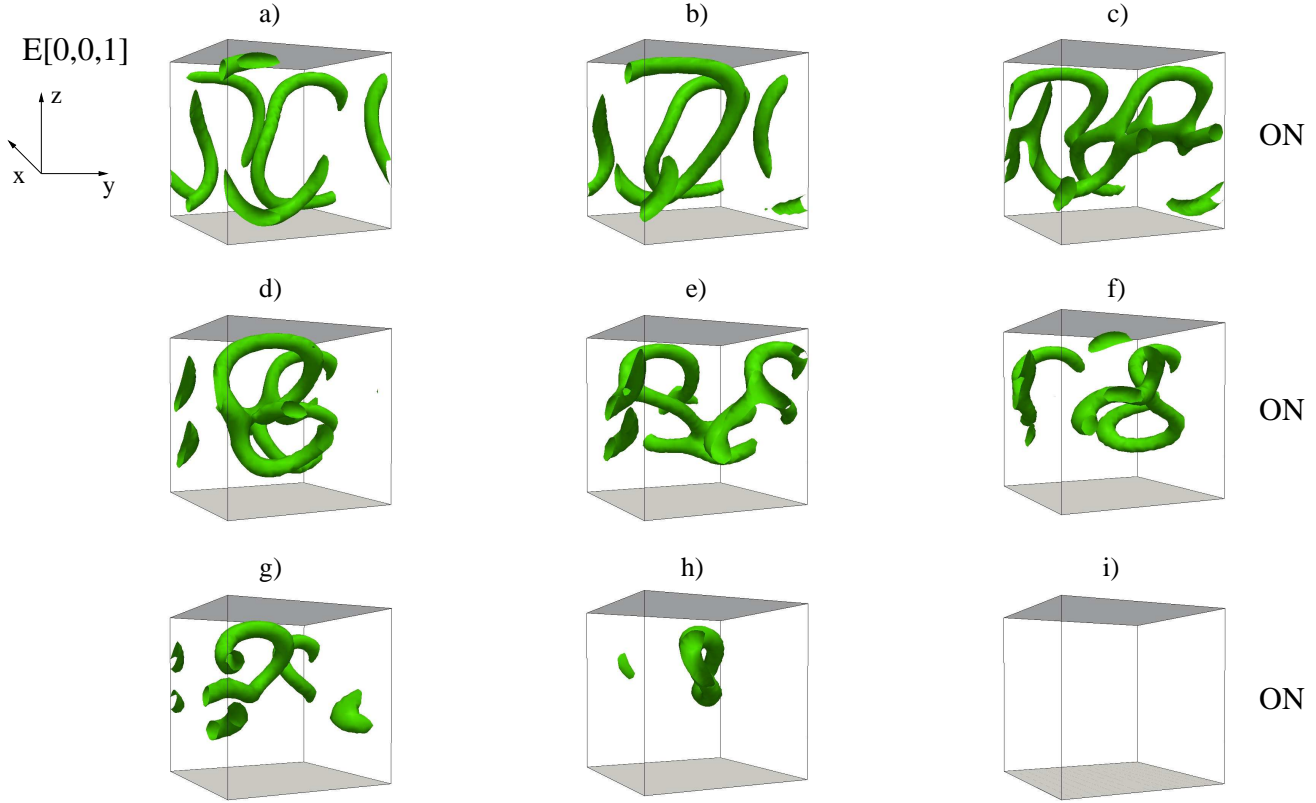


Fig. 7 Evolution of the BPI disclination network in a confined sample of size $32 \times 32 \times 32$ with homogeneous anchoring. Top and bottom walls (in grey) are oriented in the xy plane. The switching on is from *a*) to *f*) and the switching off is from *g*) to *l*). The field, applied along the z -direction ($[0,0,1]$), is such that $\mathcal{E}_{fl}^b \simeq 1$. It is switched off at $t = 128 \times 10^4$. Twisted ring defects are recognisable during the switching on, while a novel metastable state *l*), with arcs of defects spanning the device, is obtained when the field is removed.



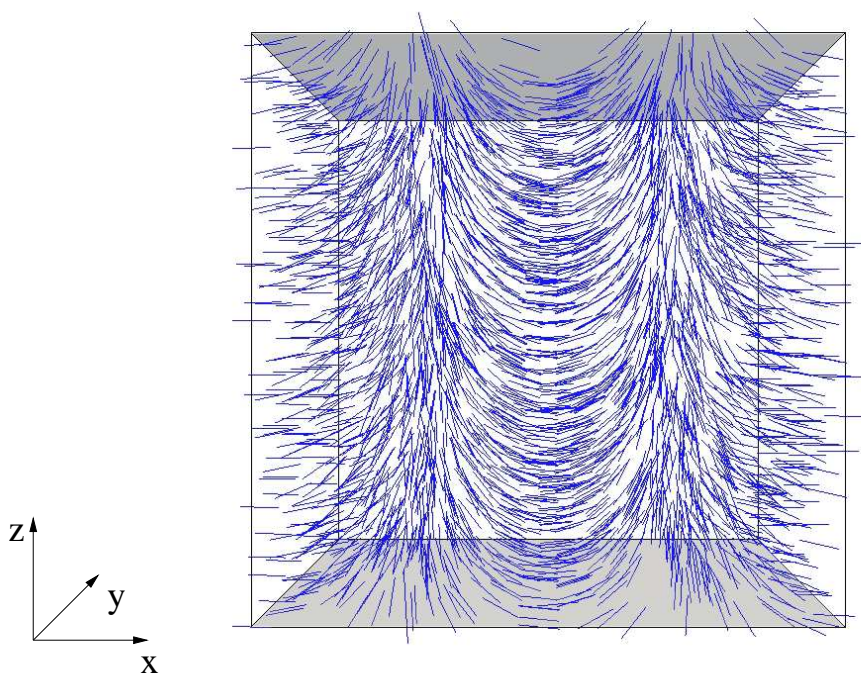


Fig. 9 3D director profile of the field-induced defect-free state in Fig. 8i.

face flexoelectric contributions, relevant at low to intermediate anchoring strength, can drive the device into yet more configurations, such as a strongly splayed-bent nematic conformation (see Fig. 9).

Our results give, we believe, a convincing demonstration that flexoelectricity and geometry are important factors in selecting defect networks in blue phases. Given the importance of flexoelectric coefficients in the materials used to build the new blue phases used in Ref.³, we hope our results will be useful when designing new blue phase-based liquid crystal devices.

Acknowledgements

We thank EPSRC EP/J007404 for funding. MEC holds a Royal Society Research Professorship.

References

- 1 H. Kikuchi, M. Yokota, Y. Hisakado, H. Yang and T. Kajiyama, *Nat. Mater.* **1** 64 (2002).
- 2 Y. Hisakado, H. Kikuchi, T. Nagamura and T. Kajiyama, *Adv. Mat.* **17** 96 (2004).
- 3 H. J. Coles and M. N. Pivnenko, *Nature* **436**, 997 (2005).
- 4 F. Castles, F. V. Day, S. M. Morris, D-H. Ko, D. J. Gardiner, M. M. Qasim, S. Nosheen, P. J. W. Hands, S. S. Choi, R. H. Friend and H. J. Coles, *Nat. Mat.* **11**, 599 (2012).
- 5 E. Karatairi, B. Rozic, Z. Kutnjak, V. Tzitzis, G. Nounesis, *Phys. Rev. E*, **81** 041703 (2010).
- 6 www.physorg.com/news129997960.html (2008).
- 7 C. Denniston and J. M. Yeomans, *Phys. Rev. Lett.* **87**, 275505 (2001); A. Tiribocchi, G. Gonnella, D. Marenduzzo, and E. Orlandini *Appl. Phys. Lett.* **97**, 143505 (2010).
- 8 H. J. Coles, M. J. Clarke, S. M. Morris, B. J. Broughton, and A. E. Blatch, *J. Appl. Phys.* **99**, 34104 (2006).
- 9 F. Castles, S. M. Morris, E. M. Terentjev, and H. J. Coles, *Phys. Rev. Lett.* **104**, 157801 (2010).
- 10 O. Henrich, D. Marenduzzo, K. Stratford, M. E. Cates, *Phys. Rev. E* **81**, 031706 (2010).
- 11 M. E. Cates, O. Henrich, D. Marenduzzo, K. Stratford, *Soft Matter* **5**, 3791-3800 (2009).
- 12 A. Tiribocchi, G. Gonnella, D. Marenduzzo and E. Orlandini, *Phys. Rev. E* **81**, 031706 (2010).

-
- dini, *Soft Matter* **7**, 3295 (2011).
- 13 O. Henrich, K. Stratford, D. Marenduzzo, M. E. Cates, *Proc. Natl. Acad. Sci. USA* **107**, 13212 (2010); O. Henrich, K. Stratford, M. E. Cates, and D. Marenduzzo, *Phys. Rev. Lett.* **106**, 107801 (2011).
 - 14 A. Tiribocchi, G. Gonnella, D. Marenduzzo, E. Orlandini, F. Salvatore, *Phys. Rev. Lett.* **107**, 237803 (2011).
 - 15 A. N. Beris, B. J. Edwards, *Thermodynamics of Flowing Systems*, Oxford University Press, Oxford (1994).
 - 16 D. C. Wright, N. D. Mermin, *Rev. Mod. Phys.* **61**, 385 (1989) and references therein.
 - 17 P. G. de Gennes and J. Prost, *The Physics of Liquid Crystals*, 2nd Ed., Clarendon Press, Oxford (1993).
 - 18 S. Chandrasekhar, *Liquid Crystals*, Cambridge University Press, (1980).
 - 19 G. P. Alexander, J. M. Yeomans, *Phys. Rev. Lett.* **99**, 067801 (2007).
 - 20 D. Marenduzzo, E. Orlandini, J. M. Yeomans, *Phys. Rev. Lett.* **92**, 188301 (2004).
 - 21 H. Grebel, R. M. Hornreich, and S. Shtrikman, *Phys. Rev. A* **28**, 1114 (1983).
 - 22 A. Dupuis, D. Marenduzzo, J. M. Yeomans, *Phys. Rev. E* **71**, 011703 (2005).
 - 23 G. P. Alexander, J. M. Yeomans, *Liq. Cryst.* **36**, 1215-1227 (2009).
 - 24 A. Dupuis, D. Marenduzzo, E. Orlandini, J. M. Yeomans, *Phys. Rev. Lett.* **95**, 097801 (2005).
 - 25 A. G. Xu, G. Gonnella and A. Lamura, *Physica A* **362**, 42 (2006).
 - 26 A. Tiribocchi, N. Stella, G. Gonnella, A. Lamura, *Phys. Rev. E* **80**, 026701 (2009).
 - 27 G. Gonnella, A. Lamura, A. Piscitelli and A. Tiribocchi, *Phys. Rev. E* **82**, 046302 (2010).
 - 28 D. Marenduzzo, E. Orlandini, M. E. Cates, J. M. Yeomans, *Phys. Rev. E* **76**, 031921 (2007).
 - 29 G. P. Alexander, J. M. Yeomans, *Phys. Rev. E* **74**, 061706 (2006).
 - 30 J. Fukuda, M. Yoneya, and H. Yokoyama, *Phys. Rev. E* **80**, 031706 (2009).
 - 31 R. M. Hornreich, M. Kugler, S. Shtrikman, *Phys. Rev. Lett.* **54**, 2099 (1985).
 - 32 J. Fukuda, S. Zumer, *Phys. Rev. Lett.* **104**, 017801 (2010).
 - 33 J. Fukuda, S. Zumer, *Phys. Rev. Lett.* **106**, 097801 (2011).
-